Title
ZnO functionalization of multiwalled carbon nanotubes for methane sensing at single parts per million concentration levels

Journal
Journal of Vacuum Science & Technology B Nanotechnology and Microelectronics Materials Processing Measurement and Phenomena, 33(6)

ISSN
2166-2746

Authors
Humayun, Tanim
Divan, Ralu
Stan, Liliana
et al.

Publication Date
2015-11-01

DOI
10.1116/1.4931694

Peer reviewed

ZnO functionalization of multiwalled carbon nanotubes for methane sensing at single parts per million concentration levels

Md Tanim Humayun, Ralu Divan, Liliana Stan, Ashu Gupta, Daniel Rosenmann, Lara Gundel, Paul A. Solomon, and Igor Paprotny

Citation: Journal of Vacuum Science & Technology B, Nanotechnology and Microelectronics: Materials, Processing, Measurement, and Phenomena **33**, 06FF01 (2015);

View online: https://doi.org/10.1116/1.4931694

View Table of Contents: http://avs.scitation.org/toc/jvb/33/6

Published by the American Vacuum Society

ZnO functionalization of multiwalled carbon nanotubes for methane sensing at single parts per million concentration levels

Md Tanim Humayun
Department of Electrical and Computer Engineering, University of Illinois at Chicago, Chicago, Illinois 60607

Ralu Divan and Liliana Stan
Center for Nanoscale Materials, Argonne National Laboratory, Argonne, Illinois 60439

Ashu Gupta
Illinois Mathematics and Science Academy, Aurora, Illinois 60506

Daniel Rosenmann
Center for Nanoscale Materials, Argonne National Laboratory, Argonne, Illinois 60439

Lara Gundel
Lawrence Berkeley National Laboratory, Berkeley, California 94720

Paul A. Solomon
U.S. Environmental Protection Agency, Las Vegas, Nevada 89199

Igor Paprotny[a)]
Department of Electrical and Computer Engineering, University of Illinois at Chicago, Chicago, Illinois 60607

(Received 27 June 2015; accepted 14 September 2015; published 23 September 2015)

This paper presents a novel atomic layer deposition (ALD) based ZnO functionalization of surface pretreated multiwalled carbon nanotubes (MWCNTs) for highly sensitive methane chemoresistive sensors. The temperature optimization of the ALD process leads to enhanced ZnO nanoparticle functionalization and improvement in their crystalline quality as shown by energy dispersive x-ray and Raman spectroscopy. The behavior of ZnO–MWCNT sensors in presence of methane concentrations down to 2 ppm level has been compared with that of pristine MWCNTs demonstrating that ZnO functionalization is an *essential* factor behind the highly sensitive chemoresistive nature of the ZnO–MWCNT heterostructures. The sensor is currently being tested under a range of conditions that include potentially interfering gases and changes to relative humidity. © *2015 American Vacuum Society*. [http://dx.doi.org/10.1116/1.4931694]

I. INTRODUCTION

Methane (CH_4) is a potent greenhouse gas with the 100-year global warming potential 28–36 times higher than that of CO_2.[1] Since 2012, U.S. has been the world-leading producer of natural gas.[2] The rapidly expanding natural gas infrastructure in the U.S. dictates the need for ubiquitous distributed low-cost methane sensors, as current CH_4 sensors suffer from low accuracy, high cost, and high power consumption. Existing metal-oxide CH_4 sensors are highly power consuming, have high detection limit (low sensitivity), and low selectivity.[3–9] Infrared absorption-based CH_4 sensors have low sensitivity and selectivity.[10] Cavity ring-down spectroscopy sensors are expensive and large, and not suitable for *in situ* leak detection.[11] The development of low power, sensitive (1 ppm), selective, and low cost CH_4 sensor is critical for enabling ubiquitous deployment throughout the natural gas infrastructure to measure and mitigate methane emissions.

Microfabricated methane sensors are promising due to their potential robustness, low power requirements, rapid response, high sensitivity, low limit of detection, stability, and low cost batch fabrication techniques. Metal-oxides, such as zinc oxide (ZnO),[4] tin oxide (SnO_2),[5] and indium oxide (In_2O_3),[6] both in bulk and nanoscale form, have been used to build microfabricated low-cost methane sensors. Most methane sensors operate on the principle of relative resistance change in presence of the target gas (i.e., chemoresistor).[3–9] However, currently available inexpensive metal oxide based chemoresistor CH_4 sensors consume significant power.[3–6]

Carbon nanotubes (CNTs) are well known for their outstanding tunable electrical properties due to their large aspect ratio (width versus length).[12,13] CNTs are essentially very long aspect ratio cylinders composed of single layers of carbon atoms, allowing most of these atoms to easily interact with surrounding gas molecules. This interaction can potentially translate to strong modulation of electrical conductance of CNTs, resulting in a large relative change in resistance, i.e., high sensitivity. In contrast with other non-CNT based electrochemical and catalytic methane sensors, CNT-based sensors have been shown to detect low concentration of target gases at room temperature, with power consumption of only a few milliwatts.[7–9] The high sensitivity, low limit of detection, low power requirements, low-cost (due to batch microfabrication process), and low sensitivity

[a)]Electronic mail: paprotny@uic.edu

to temperature variation[7–9] make CNT-based sensors potentially ideal for out-door methane sensing applications, such as distributed leak detection in natural gas pipelines.

Despite the high potential for modulating electron transport, bare CNTs are insensitive toward most target gases due to poor gas interaction of the pristine graphitic surfaces. Consequently, chemoresistive gas sensing requires either covalent (based on carboxylic acid groups) or noncovalent (based on supramolecular complexation) functionalization of CNTs with analyte-specific entities to enable modulation of their electrical properties in the presence of a target gas.[3]

Atomic layer deposition (ALD) allows precise, uniform, and conformal deposition of oxide coatings on geometrically complex substrates such as multiwalled carbon nanotubes (MWCNTs),[8,14] enabling their noncovalent functionalization. In particular, ZnO nanoparticles have been previously reported as a promising methane sensing materials[4,15] and promote energetically favorable electron transport at the ZnO–MWCNT (Ref. 16) junction compared with previously reported Pd–MWCNT.[7] Consequently, ZnO functionalizing material was suggested for surface pretreated MWCNTs. Three key factors make ZnO–MWCNT heterostructures one of the most attractive chemoresistive sensors for parts per million level CH_4 detection: (1) strong relative resistance change of ZnO nanoparticles to low concentration level of CH_4; (2) energetically favorable electron transport at ZnO–MWCNT junction, and; (3) strong electrical current modulation potential due to ballistic transport of electrons through the MWCNTs. This paper focuses on the design and fabrication of a methane sensor based on MWCNTs functionalized with ZnO deposited by ALD. The remainder of the paper is structured as follows: Section II describes the fabrication and functionalization of the MWCNT-based methane sensors. The experimental setup used to conduct the methane exposure experiments is described in Sec. III. Section IV describes the experimental results, among other the resistance change down to 2 ppm level of CH_4 at room temperature. Finally, concluding remarks are offered in Sec. V.

II. FABRICATION

The fabrication of the ZnO–MWCNT methane sensors is presented in Fig. 1. A 1 μm thick SiO_2 layer was grown on Si (100) wafers using wet oxidation at a temperature of 1100 °C for 3 h. [Fig. 1(a)]. Following the growth of the oxide layer, a set of interdigitated gold (Cr/Au) electrodes were fabricated on the SiO_2 coated Si wafer implementing a lift-off based photolithography technique [Figs. 1(b)–1(f)]. A bilayer of microchem lift-off resist 3A (LOR 3A) and S1813 photoresists was spin-coated on the SiO_2/Si wafer while a direct laser writer (LW 405) was used to do the optical exposure [Figs. 1(b) and 1(c)]. After the development process [Fig. 1(d)], a 100 nm Au film on top of a 10 nm Cr layer was deposited on the patterned photoresist using PVD 250 Lesker e-beam evaporator [Fig. 1(e)]. Deposited metal was "lifted off" by ultrasonicating the samples immersed in an 1165 remover bath [Fig. 1(f)]. Gaps between the interdigitated electrodes varied in the range of 5–10 μm (Fig. 2).

A batch of 98% pure MWCNT with 12 nm average diameter, 10 μm average lengths, and a specific surface area of ~220 m^2/g was purchased from Sigma Aldrich. An ultrasonicated solution of 1 mg/50 ml of MWCNT/ethanol was used to produce well dispersed CNT mesh. Using a microsyringe, a volume of 50 μl aliquot was deposited on a 1 mm^2 active area of the fabricated metal electrodes, which was followed by baking at 75 °C to remove the solvent and to improve adhesion [Fig. 1(g)].

The deposited MWCNTs were O_2 plasma or UV-O_3 treated inside a reactive ion etching chamber (March RIE) and a UV-O_3 chamber (Nanonex Ultra-100), respectively, for durations varying from 5 to 60 min [Fig. 1(h)]. The ALD

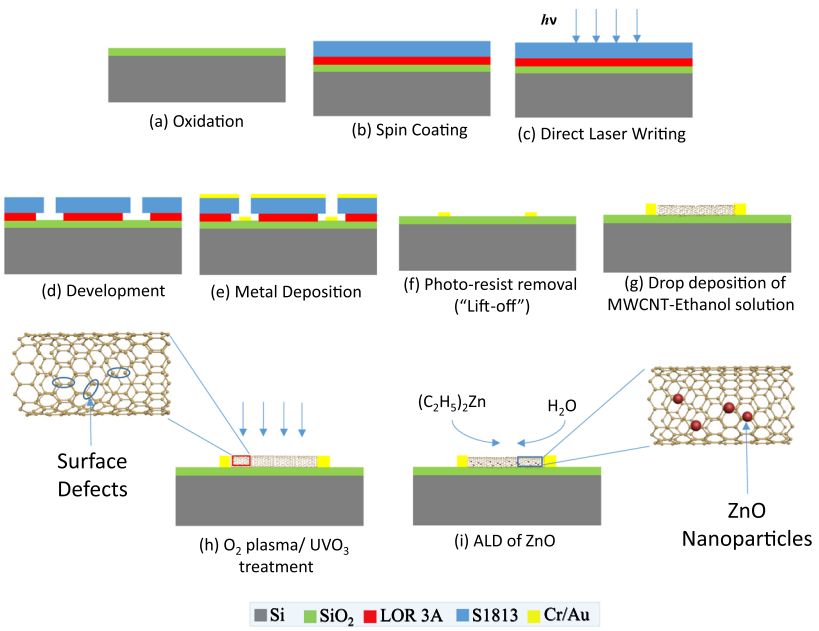

FIG. 1. (Color online) Schematic of the fabrication process of surface pretreated ZnO functionalized MWCNT methane sensor.

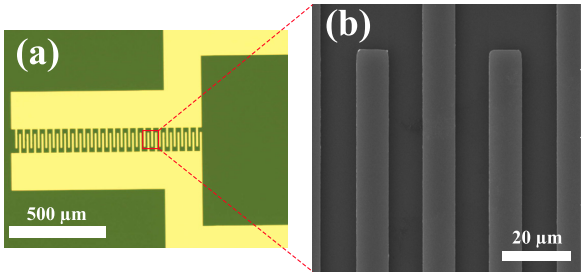

FIG. 2. (Color online) (a) Optical microscopy image of photolithography based microfabricated interdigitated Au electrodes. (b) SEM image magnifying the same electrodes.

method was used to integrate ZnO nanoparticles with surface pretreated MWCNTs. Using diethylzinc (DEZ), $[(C_2H_5)_2Zn]$, as a precursor, the ALD of ZnO (Arradiance Gemstar) on the surface pretreated MWCNTs was performed at various temperatures, from 175 to 220 °C [Fig. 1(i)]. The deposition process consists of 48 cycles. The exposure time for both DEZ and water vapor was 22 ms. The ALD process resulted in a deposition of ZnO nanoparticles from 7.74 to 10.8 nm in size on the MWCNT surface, which was confirmed by transmission electron microscopy.

The electrical conductivity of the fabricated electrodes, the CNT-deposited resistive network and ALD functionalized MWCNTs devices were measured using a digital multimeter (Fluke 115). Parasitic and contact resistance was on the order of single-digit ohm values and considered insignificant compared to the resistance of the chemoresistor (100 Ω–5 MΩ).

VEGA 3 (Tescan) scanning electron microscope (SEM) was used to characterize the ZnO functionalized MWCNTs. It was also used to perform the energy dispersive x-ray (EDX) on the ZnO–MWCNT samples. A micro-Raman system (Renishaw Invia) was used to perform green laser (wavelength of 514 nm) Raman spectroscopy on the ZnO functionalized MWCNT samples at room temperature. The power of the incident laser and acquisition time for the Raman signal were kept constant while samples fabricated under various conditions were characterized. Conditions included O_2 plasma or UV-O_3 treated MWCNT over a range of times and varying the temperature of the deposition process.

III. EXPERIMENTAL SETUP

ZnO–MWCNT sensors were tested in a sealed test chamber connected with gas inlets and electrical feedthroughs. (Fig. 3 shows a schematic of the test setup.) The residence time of the chamber was 4.5 min at the flow rate of 0.94 l/min. Relative humidity (RH) and temperature inside the test chamber were continuously monitored and recorded by a commercial data-logger (HOBO U-10 series). A computer with the help of a custom interface circuit and an analog-to-digital converter recorded real-time electrical signals generated from the sensors. A mixture of 10 ppm methane in dry air (Praxair, Inc.) was introduced to the chamber at a constant flow rate (0.94 l/min) monitored by a rotameter for

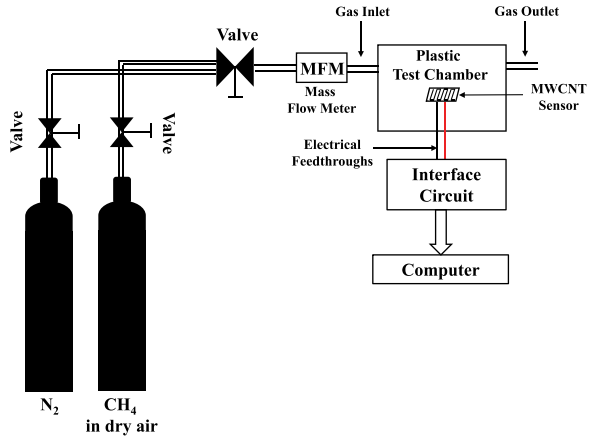

FIG. 3. (Color online) Schematic of the experimental system used to test the ZnO–MWCNTs sensor with CH_4 in dry air. N_2 was used to flash the test chamber so that the sensors can recover after each cycle of exposure to the CH_4 in dry air mixture.

30 min. The relative humidity inside the test chamber was kept constant, confirmed by a data-logging humidity sensor (HOBO U-10 series). Dry N_2 was used to purge CH_4 from the chamber and to recover the devices to their baseline resistance after each cycle of CH_4 exposure. In order to verify the detection limit at low CH_4 concentration, the change in electrical resistance of the sensors was also monitored while they were placed inside a plastic glove box filled with 2 ppm of CH_4 in ambient air mixture. A commercial CH_4 detector (Tpi 721) confirmed the concentration level of CH_4.

IV. RESULTS AND DISCUSSION

In order for the MWCNT network to function as a chemoresistor, it is necessary that the ALD-deposited ZnO does not create a direct conductive path between the electrodes outside of the MWCNT mesh, i.e., the sensor electrodes are *only* connected via the MWCNT network. This was confirmed by electrical testing; depending on the structure of the interdigitated metal electrodes and the density of the deposited MWCNT in ethanol solution, the resistance of the MWCNT-connected electrodes in our sensors varied between 100 Ωs and 5 MΩs, while the resistance outside of the MWCNT mesh was found to be infinite.

The resistances of six of our MWCNT sensors, before and after the ZnO deposition by ALD, are presented in Table I. The results show very little change (around 10% on an average) in the resistance value before and after the ALD process. The ALD process was optimized for CNT functionalization, and thus, the deposited ZnO creates a discontinuous layer that is not electrically conductive. This was verified by depositing ZnO on interdigitated Au electrodes only (not on CNTs). The resulting nonconductive 8 nm thick ZnO film (48 cycles of

TABLE I. Resistances of the sensors before and after the ZnO ALD.

Sensor #	1	2	3	4	5	6
Before ZnO deposition (Ω)	468.8	1.67	445	585.6	563.9	147 K
After ZnO deposition (Ω)	414.8	1.68	394.7	515.1	555	141 K

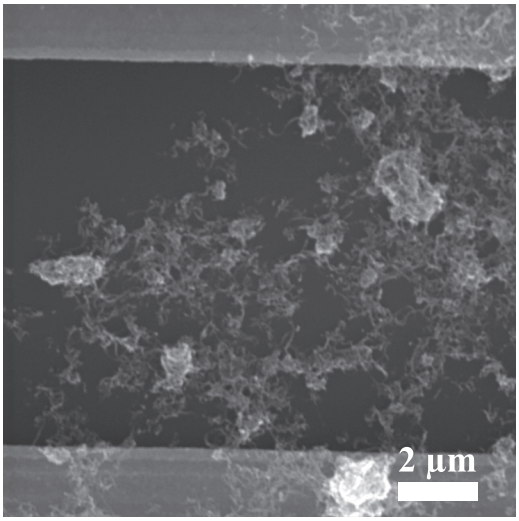

FIG. 4. SEM image of MWCNTs mesh confined between two Au electrodes.

ALD) confirmed that CNTs are an essential constituent of the sensor element.

SEM images corroborated that the functionalized MWCNTs were in proper contact with the interdigitated Au metal pads (Fig. 4). SEM and EDX results show that ZnO nanoparticles were only deposited on the active sites of the MWCNTs surface rather than on the SiO_2 surface (Fig. 5). The ZnO deposition on the active sites was enhanced as the ZnO ALD functionalizing temperature was increased from 175 to 220 °C.

Two different approaches were used to pretreat the surface of the MWCNTs before the ZnO ALD: (1) UV-O_3 and (2) O_2 plasma. Both pretreatments were found to strengthen

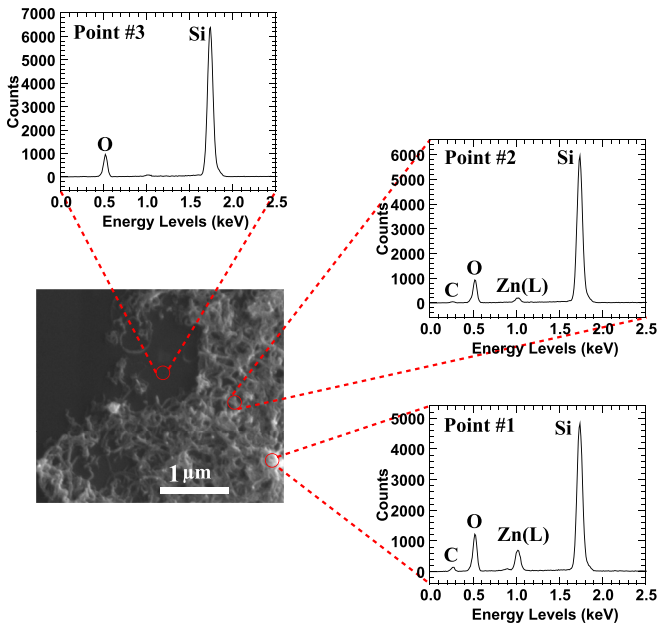

FIG. 5. (Color online) SEM and EDX results obtained from a UV-O_3 treated ZnO-functionalized MWCNT sample fabricated by ALD at 220 °C. The strong peak of the *L*-line of Zn was only found on the MWCNT (brighter point 1). Relatively weaker peak of Zn was found on less brighter point 2. Point 3, which is on the SiO_2 substrate, did not show a Zn signal.

the affinity among the MWCNT surface and functionalizing ZnO nanoparticles.

Raman spectroscopy of ZnO–MWCNT samples showed the characteristic Raman peaks (*D*, *G*, and *G*′) originating from the MWCNTs,[17] as well as characteristic Raman peaks of ZnO [$E_2^{high} - E_2^{low}$, E_2^{high} and A_1 (LO)][17,18] (Fig. 6). As seen in Figs. 6(a)–6(c), the ZnO modes were sharper and stronger at the higher temperature ALD grown samples in comparison with those originating at the lower temperatures. Based on the literature, the Raman frequency shift in the range of 566.51–574.92 cm^{-1}, for various samples processed under different conditions, is denoted as the A_1 (LO) peak of ZnO.[17,19] A Raman frequency shift in the range of 424–435.97 cm^{-1} is regarded as E_2^{high}, while in the range of 320.79–329.44 cm^{-1} is regarded as $E_2^{high} - E_2^{low}$ peak of ZnO.[17,19] Raman peaks for different samples grown under different ALD temperatures are summarized in Table II, which shows that the $E_2^{high} - E_2^{low}$ peak is not present in the Raman spectra of 175 °C ALD sample. Furthermore, in the Raman spectra of 175 °C ALD samples, the E_2^{high} and A_1 (LO) peaks are very weak in comparison with those for samples grown at 200 and 220 °C ALD.

The broadening of Raman peaks in ZnO nanoparticles compared to bulk ZnO crystals has been attributed to the confinement of optical phonons, oxygen deficiencies, and residual stress in the ZnO nanoparticles.[20] The Raman results presented in Fig. 6 and Table II demonstrate that as the ZnO ALD temperature increases, the aforementioned three phenomena becomes less prominent, indicating that the ZnO crystal quality is enhanced.

Superior crystal quality of the functionalizing ZnO nanoparticles enhances the electron transport in the MWCNT–ZnO junction,[16] thus have positive impact on the sensor performance with respect to relative resistance change, i.e., sensitivity. It is important to ensure the chemical stability and robustness of the functionalizing material so that the sensor operates accurately in harsher environments.[3] High crystal quality of the functionalizing nanomaterials helps maintain less cross-sensitivity and better reversibility as the sensor undergoes aging.[3,21] However, we were only able to test the sensitivity of 175 °C ALD samples, as the adhesiveness of the Au metal pads to external metal wires degrades significantly at higher ALD temperatures (and superior ZnO crystal quality, the phenomenon is illustrated in Fig. 7). We are currently developing a shadow mask based technique to overcome this issue.

The ZnO-functionalized MWCNT network exhibits significant resistance change when exposed to Methane even at a low concentration. The data presented in Figs. 8(a) and 8(b) were obtained from ZnO–MWCNT sensors kept in a plastic chamber and exposed to a continuous flow of a certified premixed calibration gas containing 10 ppm CH_4 in dry air (supplied by Praxair, Inc.).

The experiments were conducted at constant RH. Figure 8(a) shows the relative resistance [$\Delta R/R = (R_{methane} - R_{air})/R_{air}$] of the ZnO–MWCNT sensors (5 min O_2 plasma-treatment and ZnO ALD at 175 °C) increases monotonically while being exposed to 10 ppm of CH_4 in dry air at a constant flow rate (0.94 l/min), and reproducibly returns back to the original

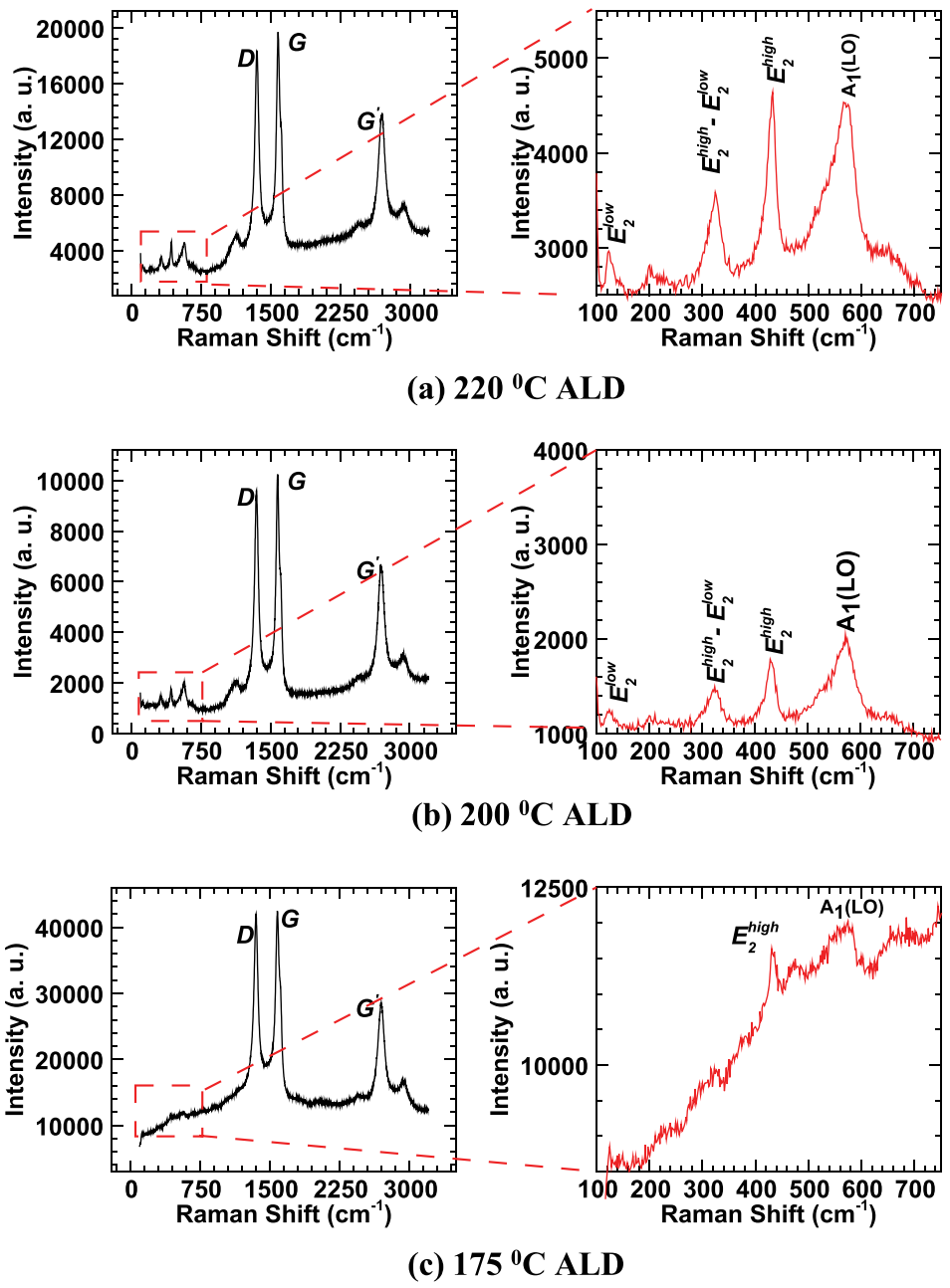

FIG. 6. (Color online) Raman spectra obtained from the ZnO–MWCNT samples at ALD temperatures of (a) 220 °C, (b) 200 °C, and (c) 175 °C. The peaks at 200.6, 429.13, 572.2, and 329.44 cm^{-1} correspond to $2E_2^{low}$, E_2^{high}, A_1 (LO), $E_2^{high} - E_2^{low}$ modes of ZnO, respectively.

levels when purging the test chamber with N_2. No response to CH_4 was observed for sensors fabricated with nonfunctionalized MWCNTs [Fig. 8(b)], corroborating our hypothesis that the change in resistance is caused by the transfer of electrons from the MWCNT surface to the intermediate complex generated by the ZnO nanoparticles and CH_4 molecules. No change in resistance was observed in nonpretreated but functionalized MWCNTs, indicating that the surface pretreatment is an important component of CNT functionalization. The best relative resistance change for the ZnO–MWCNTs sensors at 10 ppm of CH_4 in dry air was found to be 12.1% on an average with a standard deviation of 2.11%.

Figure 8(c) presents the change in electrical resistance of our ZnO–MWCNT sensors exposed to 2 ppm CH_4 in ambient

TABLE II. Frequency shift originating from different ZnO Raman modes for ZnO nanoparticles deposited at different ALD temperatures on the MWCNTs.

ALD temperature (°C)	$E_2^{high} - E_2^{low}$ peak position (cm^{-1})	E_2^{high} peak position (cm^{-1})	A_1 (LO) peak position (cm^{-1})
175	Mostly absent	430.78–431.5 (weaker)	568.84–574.86 (weaker)
200	329.44	424–429.13	564.82–571.55
220	320.79–327.71	430.84–435.97	566.51–574.92

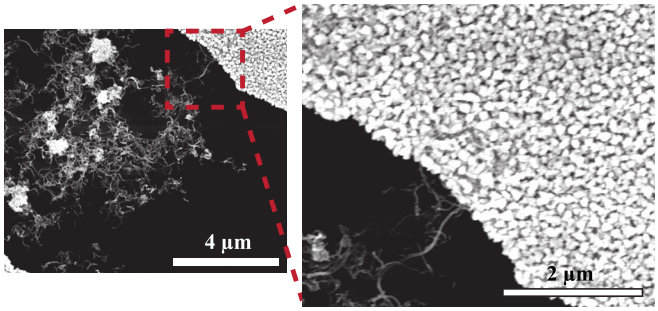

FIG. 7. (Color online) SEM images of a ZnO–MWCNTs sensor with the ALD temperature at 220 °C. Inset shows the change in texture of the interdigitated Au electrodes due to the high (220 °C) temperature during the ALD process.

air while in a sealed plastic glove box, indicating the lower detection limit of our sensor [see Fig. 8(c)]. The commercial reference sensor used in this experiment (Tpi 721, manufactured by Test Products Int.) only provides accurate data under static conditions (i.e., no flow) since it is highly sensitive to surrounding gas flow.[22] The metal oxide based microfabricated chemoresistor (Figaro 2611, manufactured by Figaro USA, Inc.) in the Tpi 721 commercial sensor has a high relative power requirement limiting its use, e.g., when power is not available or many measurements are required.

ZnO functionalized CNT based chemoresistor sensors are sensitive to CO (Ref. 23) and NO_2.[24] H_2O, O_2, and H_2 are also possible interfering gases.[25] To study the effect of RH on sensor performance, the resistance change of the ZnO–MWCNT sensors for different RH was measured at room temperature using controlled flow of moist air inside an enclosed plastic chamber. The resistance of the sensor showed a reversible change as the RH was increased from 10% to 91% and reduced back to 10%. The highest recorded relative resistance change $[(R_{water} - R_{air})/R_{air}]$ for the ZnO–MWCNT sensor was almost 4% at 91% RH.

We also performed several preliminary tests with CO_2; however, further experiments are required to confirm potential sensitivity. Future plans include exposing the sensor to CO_2, H_2, and O_2 to map sensitivity to these interfering gases.

V. CONCLUSIONS

A methane sensor has been developed which is able to detect CH_4 in the low parts per million range in dry air at room temperature. It is based on MWCNTs functionalized with ZnO deposited by ALD. A surface pretreatment by O_2-plasma or UV-O_3 is essential for MWCNTs functionalization. The crystalline quality of the functionalizing ZnO material is strongly dependent on the ALD process temperature. The best sensitivity was observed with an O_2 plasma pretreated MWCNT with ZnO deposition at 175 °C. Our group continues to develop the methane sensor and test it with possible interfering gases, such as H_2O, O_2, H_2, and CO_2. We also plan to explore the effect of changes in the dimensions, morphology, and crystal quality of the functionalizing compound on the sensor response. We predict that

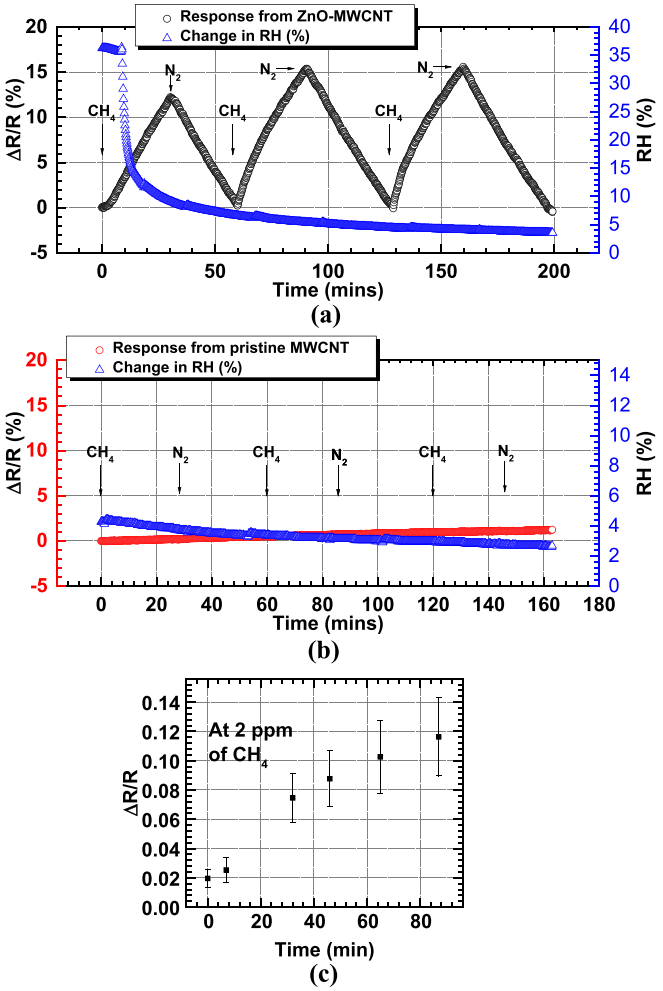

FIG. 8. (Color online) (a) Relative resistance change of the ZnO functionalized MWCNT (5 min O_2 plasma pretreated) sensor while subjected to repetitive exposure of 10 ppm of CH_4 in dry air and N_2. (b) Relative resistance change of the pristine MWCNT while subjected to repetitive exposure of 10 ppm of CH_4 in dry air and N_2. Right hand y-axes in both plots show change in RH (%) inside the test chamber during the tests. (c) Relative resistance change of the ZnO–MWCNT sensor while exposed to 2 ppm concentration of CH_4 in air.

the functionalized MWCNT sensor using the plasma and UV-O_3 pretreatment will result in a low power and low cost sensor able to detect methane at a parts per million or better, and useful for, e.g., distributed leak detection on natural gas infrastructures. Application of such sensor may not only have the potential to reduce methane emissions to the environment, but also help save lives by avoiding methane explosions in residential and commercial settings.

ACKNOWLEDGMENTS

The authors would like to thank David Gosztola, CNM, Argonne National Laboratory, for helping with the Raman spectroscopy. Use of the Center for Nanoscale Materials, an Office of Science user facility, was supported by the U.S. Department of Energy, Office of Science, Office of Basic Energy Sciences, under Contract No. DE-AC02-06CH11357. College of Engineering, University of Illinois, Chicago, IL, in part funded the project. The U.S. Environmental Protection

Agency, through its Office of Research and Development, collaborated in the research described here. It has been subjected to Agency review and approved for publication.

[1]United States Environmental Protection Agency, "Overview of greenhouse gases," Last accessed August 20, 2015, http://epa.gov/climatechange/ghgemissions/gases/ch4.html.
[2]U.S. Energy Information Administration, "U.S. remained world's largest producer of petroleum and natural gas hydrocarbons in 2014," Last accessed August 30, 2015, http://www.eia.gov/todayinenergy/detail.cfm?id=20692.
[3]T. Zhang, S. Mubeen, N. V. Myung, and M. Deshusses, Nanotechnology **19**, 332001 (2008).
[4]D. Barreca, D. Bekermann, E. Comini, A. Devi, R. A. Fischer, A. Gasparotto, C. Maccato, G. Sberveglieri, and E. Tondello, Sens. Actuator B **149**, 1 (2010).
[5]P. Fau, M. Sauvan, S. Trautweiler, C. Nayral, L. Erades, and A. Maisonnat, Sens. Actuator B. **78**, 1 (2001).
[6]T. Waitz, T. Wagner, T. Sauerwald, C. D. Kohl, and M. Tiemann, Adv. Funct. Mater. **19**, 653 (2009).
[7]G. Lu, L. Ocola, and J. Chen, Adv. Mater. **21**, 2487 (2009).
[8]M. Willinger, G. Neri, E. Rauwel, A. Bonavita, G. Micali, and N. Pinna, Nano Lett. **8**, 4201 (2008).
[9]Y. Lu, J. Li, J. Han, H. T. Ng, C. Binder, C. Partridge, and M. Meyyappan, Chem. Phys. Lett. **391**, 344 (2004).
[10]C. Massie, G. Stewart, G. McGregor, and J. R. Gilchrist, Sens. Actuator B: Chem. **113**, 830 (2006).
[11]United States Environmental Protection Agency, "Measurement of the carbon isotopic ratio of atmospheric methane," Last accessed August 20, 2015, http://cfpub.epa.gov/ncer_abstracts/index.cfm/fuseaction/display.abstractDetail/abstract/6351/report/0.
[12]M. S. Dresselhaus, G. Dresselhaus, and R. Saito, Carbon **33** 883 (1995).
[13]L. Valentini, I. Armentano, J. M. Kenny, C. Cantalini, L. Lozzi, and S. Santucci, Appl. Phys. Lett. **82**, 961 (2003).
[14]S. Boukhalfa, K. Evanoff, and G. Yushin, Energy Environ. Sci. **5**, 6872 (2012).
[15]P. Bhattacharyya, P. K. Basu, H. Saha, and S. Basu, Sens. Actuator B **124**, 62 (2007).
[16]H. Zhang, N. Du, B. Chen, D. Li, and D. Yang, Sci. Adv. Mater. **1**, 13 (2009).
[17]X. L. Li, C. Li, Y. Zhang, D. P. Chu, W. I. Milne, and H. J. Fan, Nanoscale Res. Lett. **5**, 1836 (2010).
[18]Y. Zhu *et al.*, Adv. Mater. **18**, 587 (2006).
[19]R. Cuscó, E. A. Lladó, J. Ibáñez, and L. Artús, Phys. Rev. B **75**, 165202 (2007).
[20]K. Alim, V. Fonoberov, M. Shamsa, and A. Balandin, J. Appl. Phys. **97**, 124313 (2005).
[21]I. Sayago *et al.*, Sens. Actuator B **122**, 75 (2007).
[22]Figaro Engineering Inc., Japan, "Application Notes TGS2611," Last accessed September 21, 2015, see http://www.datasheetarchive.com/dlmain/Datasheets-11/DSA-218253.pdf.
[23]J. Khanderi, R. Hoffmann, A. Gurlo, and J. Schneider, J. Mater. Chem. **19**, 5039 (2009).
[24]B. Albiss, W. Sakhaneh, I. Jumah, and I. Obaidat, IEEE Sens. J. **10**, 1807 (2010).
[25]O. Lupan, G. Chai, and L. Chow, Microelectron. Eng. **85**, 2220 (2008).